Influence of the Properties of Ferroelectric Liquid Crystals on the Spontaneous Polarization Reorientation Photorefractive Effect

Takeo Sasaki,* Atsushi Katsuragi, Oki Mochizuki, and Yukihito Nakazawa

Department of Chemistry, Faculty of Science, Science University of Tokyo, 1-3 Kagurazaka, Shinjuku-ku, Tokyo 162-8601, Japan

Received: April 17, 2003

The photorefractivity of 14 ferroelectric liquid crystals (FLCs) mixed with a photoconductive compound was investigated by two-beam coupling experiments. The influence of the properties of low-molecular-weight FLCs on the photorefractive effect was examined, and it was found that the photorefractive two-beam coupling gain coefficients and the refractive index grating formation time are strongly dependent on the properties of FLCs. The effects of the magnitude of the spontaneous polarization, the viscosity, and the homogeneity of the surface-stabilized state on the photorefractivities of FLCs are discussed based on these findings.

Introduction

The photorefractive effect is defined as the optical modulation of the refractive index of a medium as a result of a number of processes.[1−5] There are several phenomena in which a change in refractive index is induced by the absorption of light and include photochemical reactions, photochromism, and the photothermal effect. The photorefractive effect is a phenomenon in which the change in refractive index is induced by a combined mechanism of photovoltaic and electrooptic effects. The change in refractive index by the photorefractive effect occurs only within the interference pattern of the incident laser beams. This effect has direct applicability in photonics, including optical image processing, parallel optical logic, pattern recognition, and phase conjugation. A material that exhibits both photovoltaic and electrooptic effects is potentially usable as a photorefractive material, and inorganic transparent semiconductor crystals and organic photoconductive polymers possessing D−π−A chromophores (in which donor and acceptor groups are attached to a π-conjugate system) are well-known examples.

The interference of two laser beams in a photorefractive material establishes a refractive index grating. The mechanism responsible for the formation of this refractive index grating is the generation of a space-charge field (internal electric field) because of charge separation between bright and dark areas of interference and a subsequent change in the refractive index via an electrooptic effect (such as Pockels effect). A characteristic of the photorefractive effect is that the phase of the refractive index grating is shifted by $\pi/2$ from the interference pattern.[1−5] In such a phase-shifted index grating, laser beams undergo a unique mode of propagation. The interfering laser beams are energetically coupled in the photorefractive material through the phase-shifted index grating. The transmitted intensity of one beam through the material appears to increase, whereas that of the other appears to decrease. This phenomenon is known as asymmetric energy exchange in photorefractive two-beam coupling. The photorefractivity of a material is often evaluated based on its two-beam coupling efficiency (the coupling ratio and the gain coefficient) and the diffraction efficiency of the index grating.[3] One class of materials that exhibits high photorefractivity is glassy photoconductive polymer materials doped with high concentrations of D−π−A chromophores.[6−16] To obtain photorefractivity in polymer materials, a high electric field of 10∼50 V/μm is usually applied to the polymer film. This electric field is necessary to pole the film (activation of the Pockel effect) and to increase the charge generation efficiency. The photorefractivity of organic materials is greater than that of inorganic materials because of the ability of component D−π−A chromophores to reorientate in the internal electric field, and the photorefractive effect primarily induced by the chromophoric reorientation is known as the orientational photorefractive effect.

The photorefractive effect of low-molecular-weight nematic liquid crystals doped with photoconductive compounds has been investigated,[17−26] and the photoinduced changes in the refractive index in such liquid crystals has been shown to be caused by changes in the orientation of liquid crystal molecules because of the photoinduced internal electric field. The effect of the reorientation of liquid crystal molecules on the apparent refractive index is particularly strong. However, despite these advantages of organic photorefractive materials, their response time is too slow (usually ∼100 ms) for practical applications, attributable to the slow reorientation of chromophores.

Recently, the photorefractivity of surface-stabilized ferroelectric liquid crystals (SS−FLCs) doped with a photoconductive compound has been reported.[27−32] These FLCs are classified as smectic phase-forming LCs, and in that phase, the molecules form a layered structure. The FLCs exhibit photorefractivity only at the temperature where the LCs exhibit a ferroelectric phase (Sc* phase). FLCs have a very fast photorefractive response, and exhibit spontaneous polarization (bulk polarization) when sandwiched between flat plates of a few micrometers in thickness (surface-stabilized state[33]). The direction of spontaneous polarization is governed by the photoinduced internal electric field, giving rise to a refractive index grating with properties dependent on the direction of polarization. Figure 1 shows a schematic illustration of the mechanism of the photorefractive effect in FLCs. In this scheme, the internal electric field alters the direction of spontaneous polarization in the area between the bright and dark positions of the interference pattern, which induces a periodic change in the orientation of

* To whom correspondence should be addressed.

10.1021/jp030456d CCC: $25.00
Published on Web 07/12/2003

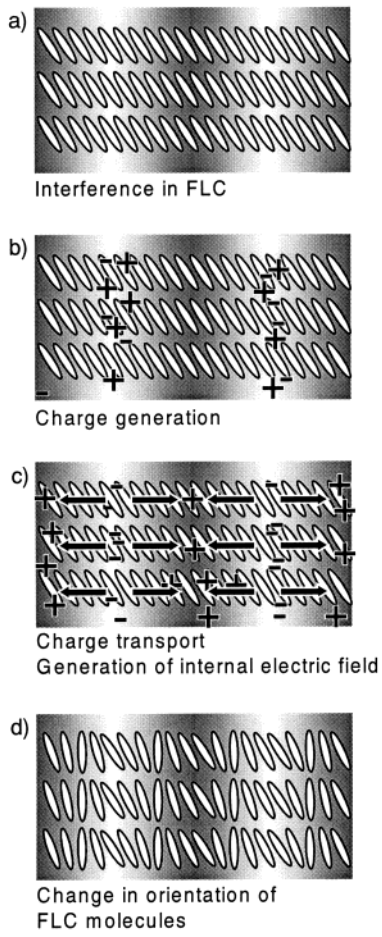

Figure 1. Schematic illustration of the mechanism of the photorefractive effect in FLCs: (a) two laser beams interfere in the surface-stabilized state of the FLC/photoconductive compound mixture; (b) charge generation occurs at the bright area of interference; (c) while electrons are trapped at the trap site in the bright area, holes migrate by diffusion or drift in the presence of an external electric field to generate an internal electric field between the bright and dark positions; (d) the orientation of the spontaneous polarization vector (i.e., orientation of mesogens) is altered by the internal electric field.

FLC molecules. This is different from the processes that occur in other photorefractive materials in that the molecular dipole, rather than the bulk polarization, responds to the internal electric field. The peculiar photorefractive behavior of FLCs is related to the properties of the FLCs themselves. Compared to nematic LCs, FLCs are more crystal than liquid, and the preparation of fine FLC films requires several sophisticated techniques. Obtaining a uniformly aligned, defect-free surface-stabilized FLC (SS−FLC) using a single FLC compound is very difficult,[34,35] and mixtures of several LC compounds are usually used to obtain fine SS−FLC films. In this study, 14 FLC mixtures with differing properties were prepared, and the effects of temperature, applied electric field, magnitude of spontaneous polarization, and homogeneity of the SS-state on the photorefractive properties of these FLCs were examined. The factors affecting the photorefractivity of FLCs were also investigated.

Experimental Section

Samples. The FLC mixtures used in this study were obtained commercially (FELIX series, Clariant Corporation), with the properties as listed in Table 1. The structures of photoconductive compounds and the sensitizer are shown in Figure 2. The photoconductive compound, CDH, was synthesized via the reaction of diphenylhydrazine and *N*-ethylcarbazole-3-carboxaldehyde in pyridine. TNF (sensitizer/electron trap reagent) was obtained from Tokyo Kasei Co. The final concentration of CDH in the film was 0∼2 wt %, and that of TNF was 0.1 wt %. The FLCs and dopants were dissolved in dichloroethane, and the solvent was evaporated. The mixture was then dried in a vacuum at room temperature for one week. The samples were injected into a 10-μm-gap glass cell equipped with 1 cm^2 ITO electrodes and a polyimide alignment layer (LX-1400, Hitachi Chemicals Co.).

Measurement. The phase transition temperatures were determined by differential scanning calorimetry (DSC; DSC20-TS15, Mettler) and microscopic observation (FP-80, FP-82, Mettler; BX-50 polarizing microscope, Olympus). The photorefractive effect was measured in a two-beam coupling experiment. A p-polarized beam from an Ar^+ laser (165LGS−S, Laser Graphics; 488 nm, continuous wave) was divided by a beam splitter and interfered in the sample film. The intensity of the laser was 2.4 mW for each beam (1 mm diameter). The laser incidence geometry is shown in Figure 2. The sample was thermostated using a thermo-controller (DB1000, Chino Co.). An electric field of 0∼10 V/μm was applied to the sample from a regulated DC power supply (Kenwood DW36-1), and the change in transmitted beam intensity was monitored by photodiodes (ET-2040, Electrooptics Technology, Inc.) and recorded by a computer. The spontaneous polarization of FLCs was measured by the triangular voltage method (10 Vp-p, 100 Hz).[33]

Results and Discussion

POM Observation of SS−FLC Samples. The textures of FLCs doped with CDH and TNF in 10-μm-gap cells were observed by polarizing optical microscopy (POM). The alignment of FLC molecules is dominated not only by the properties of FLCs but also by the affinity of FLC molecules with the alignment layer (polyimide coating). LC molecules interact with the alignment layer and form a homogeneous, anisotropic film in which the LC molecules are aligned in a specific direction. The fabrication of FLC cells (see Figure 2) involves the coating of ITO glass with polyimide, rubbing treatment of the polyimide surface, and precise assembly of those glasses into a gap in a cell of only a few micrometers in width. All of these processes affect the quality (homogeneity) of the surface-stabilized states, and the appropriate preparation conditions differ from FLC to FLC. Direct comparison of the optical properties of different FLCs is therefore very difficult. In this study, Hitachi Chemicals LX-1400 polyimide, as used industrially in nematic LC displays, was chosen for the alignment layer. The thickness of the polyimide coating was set to 20−30 nm, and the surface of the polyimide was rubbed with a polyester roll using a rubbing machine (RM-300/50, EHC Co. Ltd.) under specific conditions. All FLCs listed in Table 1 exhibited finely aligned SS states when they were not mixed with CDH and TNF. Figure 3 shows typical examples of textures observed in FLCs 017/000, M4851/050, and SCE8. As the CDH concentration increased, defects appeared in the texture. M4851/050 and SCE8 retained the SS state with few defects at CDH concentrations below 2 wt %. All FLCs used in this study, except for SCE8 and M4851/050, exhibited distorted SS states, and light scattering was very strong when mixed with CDH at concentrations higher than 0.5 wt %.

Two-Beam Coupling Experiment using FLCs. Figure 4 shows a typical example of the asymmetric energy exchange observed in the SCE8/CDH/TNF sample under an applied electric field of 0.1 V/μm. Interference of the divided beams in the sample resulted in increased transmittance of one of the

TABLE 1: Physical Properties of FLCs Used in This Study

FLC	Ps at 25 °C (nC/cm^2)	phase transition temperature[a] (°C)	response time τ[b] (μs)	rotational viscosity γ_ϕ (mPas)	tilt angle (deg)
015/000	9	- Sc* 71 S_A 83 N* 86 I	70	60	24
015/100	33	- Sc* 72 S_A 83 N* 86 I	21	80	23
016/000	−4.3	- Sc* 72 S_A 85 N* 93 I	70	61	25
016/030	−5.9	- Sc* 72 S_A 85 N* 93 I	47	82	25
016/100	−10.5	- Sc* 72 S_A 85 N* 94 I	20	60	27
017/000	9.5	- Sc* 70 S_A 76 N* 87 I	93	47	26
017/100	47	- Sc* 73 S_A 77 N* 87 I	23	116	27
018/000	23	- Sc* 65 S_A 82 N* 88 I	59	68	22
018/100	40	- Sc* 67 S_A 82 N* 89 I	30	97	23
019/000	8.3	- Sc* 60 S_A 76 N* 82 I	262	37	19
019/100	39	- Sc* 64 S_A 78 N* 87 I	53	75	20
SCE8	−4.5	- Sc* 60 S_A 80 N* 104 I	50	76	20
M4851/000	−4.0	- Sc* 64 S_A 69 N* 73 I	40		25
M4851/050	−14	- Sc* 65 S_A 70 N* 74 I	22	65	28

[a] C, crystal; Sc*, chiral smectic C phase; S_A, smectic A phase; N* chiral nematic phase; I, isotropic phase. [b] Response time to 10 V/μm electric field at 25 °C in a 2-μm cell.

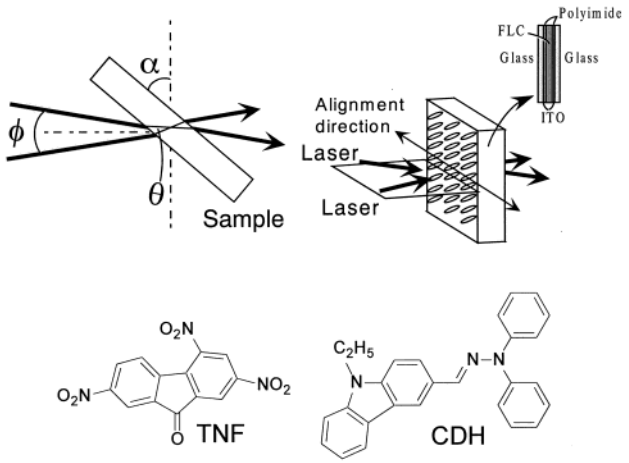

Figure 2. Beam incidence geometry and structures of photoconductive compound CDH and electron trap reagent TNF.

beams and decreased transmittance of the other beam. These transmittance characteristics were reversed when the polarity of the applied electric field was reversed. Asymmetric energy exchange was only observed when an electric field was applied, indicating that beam coupling was not caused by a thermal grating. To calculate the two-beam coupling gain coefficient, the diffraction condition needs to be correctly identified. The two possible diffraction conditions are the Bragg regime and the Raman-Nath regime, distinguished by the dimensionless parameter Q as follows:[2]

$$Q = 2\pi\lambda L/n\Lambda^2 \qquad (1)$$

where L is the interaction path length. Here, $L = 12$ μm ($\alpha = 50°$, $\phi = 20°$, $n = 1.65$). The spacing of the interference pattern (Λ) was 1.9 μm inside the material. The Bragg regime of optical diffraction is defined as $Q > 1$ and excludes multiple scattering to produce only one order of diffraction of light. Conversely, $Q < 1$ is defined as the Raman-Nath regime of optical diffraction, in which many orders of diffraction can be observed. A Q value of greater than 10 is usually required to guarantee that diffraction occurs entirely in the Bragg regime. Under the present experimental conditions, Q is calculated to be 6.2. Therefore, the diffraction observed in this experiment occurs predominantly, but not entirely, in the Bragg regime, with a small Raman-Nath component. However, because higher-order diffraction was not observed, the two-beam coupling gain coefficient Γ was calculated assuming Bragg diffraction, as follows:[1,2]

$$\Gamma = \frac{1}{L}\ln\left(\frac{gm}{1+m-g}\right) \qquad (2)$$

where g is the ratio of intensities of the signal beam behind the sample with and without a pump beam and m is the ratio of the beam intensities (pump/signal) in front of the sample.

Effect of Laser Incidence Condition. The effect of the beam incidence condition on the magnitude of the gain coefficient was investigated. The gain coefficient of SCE8 doped with 2 wt % CDH and 0.1 wt % TNF was measured as a function of sample angle α and intersection angle ϕ, as indicated in Figure 2. The dependence of the gain coefficient on the sample angle α is shown in Figure 5. The gain coefficient increased with sample angle, up to a maximum at ~60°. The length of the optical path inside the FLC film also increases with the sample angle; thus, the increase in the gain coefficient may originate from the increase in interaction path length of the beams and the increased intensity of the external electric field component along the interference wave vector (the direction of charge separation). The decrease in the gain coefficient at larger sample angles is caused by the increased reflection at the surface of the glass cell. This inset in Figure 8 shows the dependence of the gain coefficient on the intersection angle ϕ. The gain coefficient decreased with increasing intersection angle, with a corresponding narrowing of the interference pattern. The magnitude of the gain coefficient as a function of the spacing of the interference pattern (Λ) is shown in Figure 6. Thus, the dependence on the intersection angle can be attributed to the resolution of the refractive index grating.

Comparison of Photorefractive Properties of FLCs. The photorefractivities of several FLC mixtures (CS series, Chisso Chemicals) CS1011, CS1015, CS1022, and CS1030 (Table 2) doped with CDH and TNF were investigated previously.[31] All formed finely aligned SS-state domains in 10-μm-gap cells with a LX-1400 polyimide alignment layer and exhibited clear photorefractivity in the ferroelectric phase. However, in the FELIX series FLCs in this study, only 2 of the 14 FLCs exhibited clear photorefractivity using an identical cell. SCE8 and M4851/050 displayed finely aligned SS-state domains in a 10-μm-gap cell and exhibited asymmetric energy exchange. FLCs that formed an SS state with many defects did not exhibit clear asymmetric energy exchange. Figure 7 shows the results of a two-beam coupling experiment using 017/100 doped with 1 wt % CDH and 0.1 wt % TNF (the texture of this sample is

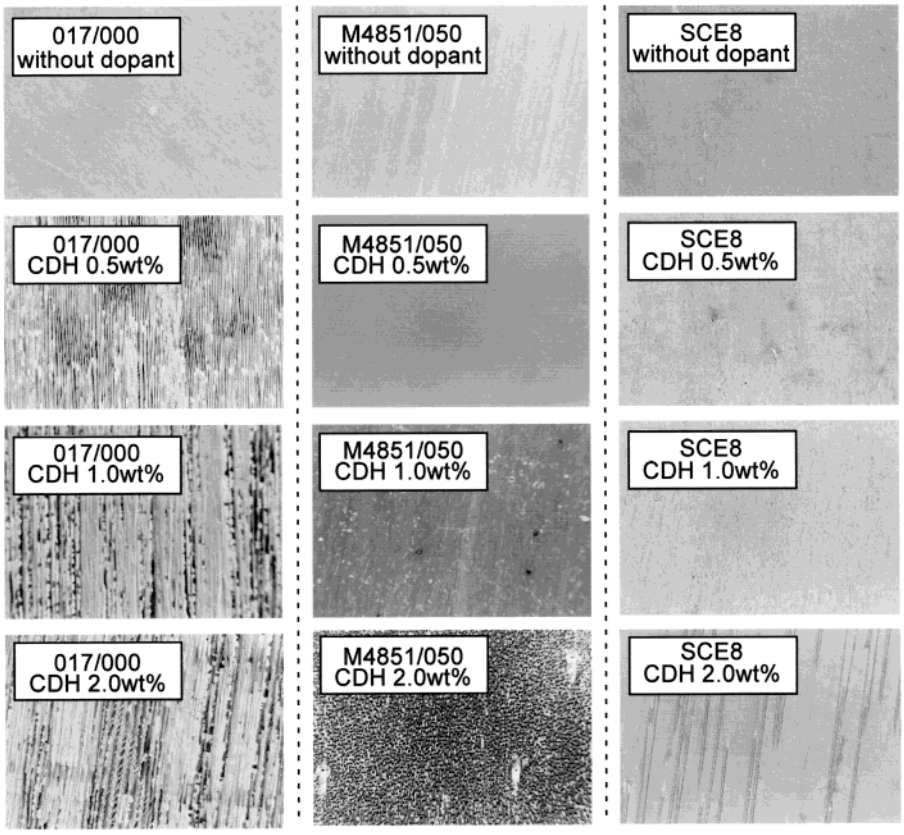

Figure 3. Textures observed by POM observation of SS states in FLCs.

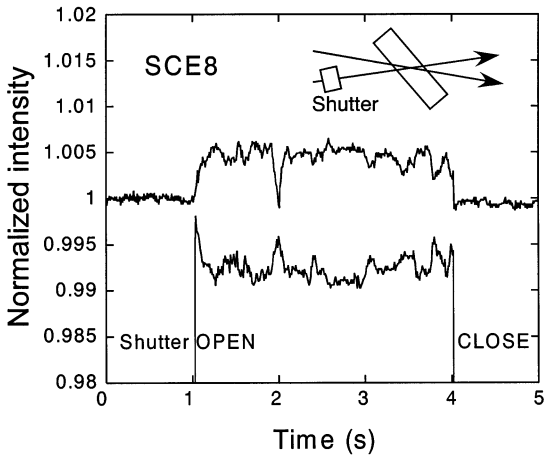

Figure 4. Typical example of asymmetric energy exchange observed in SCE8 mixed with 2 wt % CDH and 0.1 wt % TNF. The sample angle α was 50°, and the intersection angle ϕ was 20°.

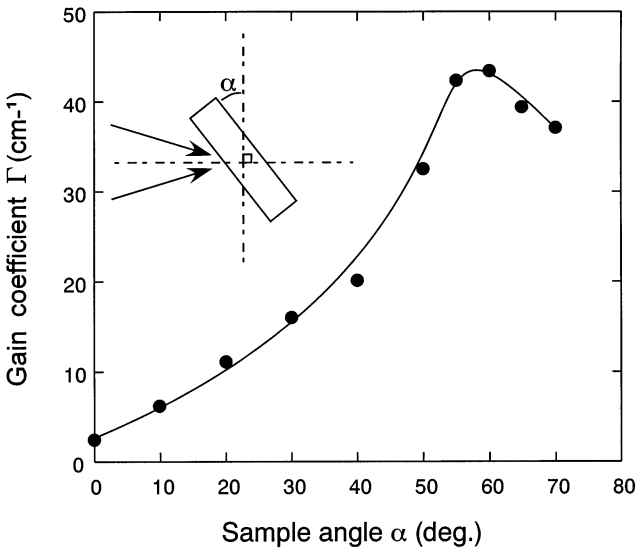

Figure 5. Gain coefficient of SCE8 mixed with 2 wt % CDH and 0.1 wt % TNF as a function of the sample angle α. The intersection angle ϕ was set to 20°.

shown in Figure 5). No asymmetric energy exchange was observed in this sample. In those distorted SS states, laser beams are strongly scattered, precluding the formation of a refractive index grating. The temperature dependence of the gain coefficient of SCE8 doped with 2 wt % CDH and 0.1 wt % TNF is shown in Figure 8a. Asymmetric energy exchange was observed only at temperatures below 46 °C. The spontaneous polarization of the SCE8/CDH/TNF mixture is plotted as a function of temperature in Figure 8b. Similarly, the spontaneous polarization vanished when the temperature was raised above 46 °C. Thus, asymmetric energy exchange was observed only in the temperature range in which the sample exhibits ferroelectric properties (Sc* phase). The temperature dependences of the gain coefficients of these SCE8 samples and the M4851/050 samples with several concentrations of CDH are shown in Figure 9.

Asymmetric energy exchange was observed only in the Sc* phase. As the CDH concentration increased, so did the gain coefficient. This may be due to increased charge mobility in the FLC medium. The highest temperature at which asymmetric energy exchange was observed became lower with decreasing Sc*−S_A phase transition temperature. Because the molecular dipole moment of FLCs is small and the dipole moment is aligned perpendicular to the molecular axis, large changes in the orientation of the molecular axis cannot be induced by the internal electric field in the S_A or N* phase of the FLCs used in this study. However, in the Sc* phase, reorientation associated with spontaneous polarization occurs because of the internal

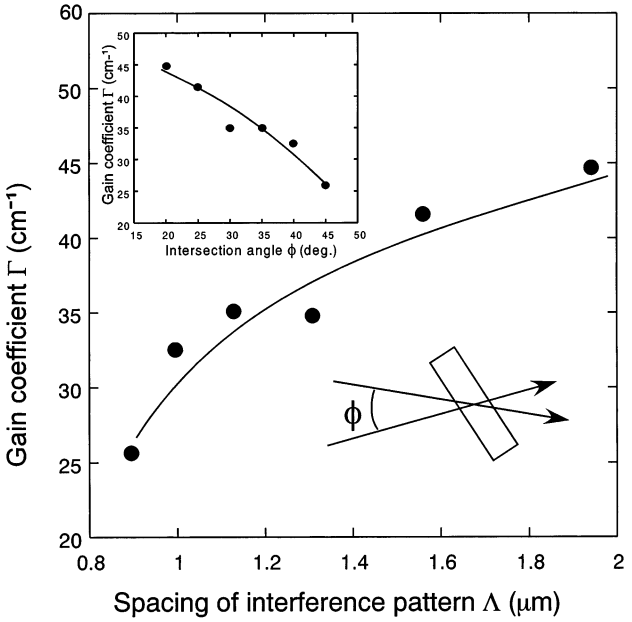

Figure 6. Gain coefficient of SCE8 mixed with 2 wt % CDH and 0.1 wt % TNF as a function of the spacing of the interference pattern Λ. Inset shows the gain coefficient as a function of the intersection angle ϕ. The sample angle α was set to 50°.

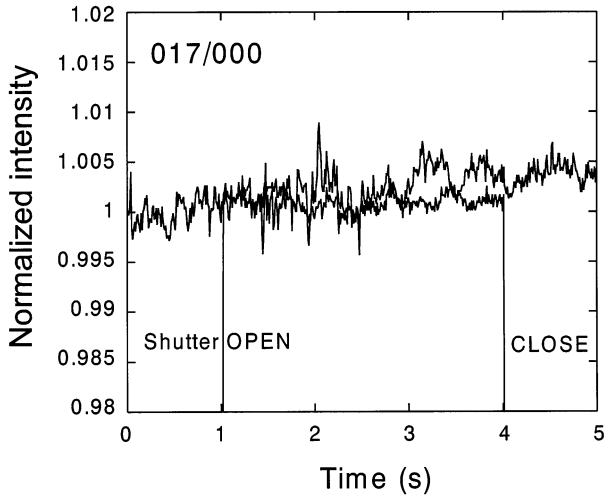

Figure 7. Example of the results of two-beam coupling experiments for 017/100 mixed with 1 wt % CDH and 0.1 wt % TNF. The sample angle α was 50°, and the intersection angle ϕ was 20°.

TABLE 2: Physical Properties of FLCs Used in the Previous Study[26]

FLC	Ps at 25 °C (nC/cm²)	phase transition temperature[a] (°C)	response time τ[b] (μs)	tilt angle (deg.)
CS1011	13.0	- Sc* 56 S_A 77 N* 91 I	899	22
CS1015	6.6	C −17 Sc* 58 S_A 68 N* 78 I	188	26
CS1022	34.7	C −11 Sc* 61 S_A 73 N* 85 I	56	25
CS1030	20.2	C −5 Sc* 70 S_A 74 N* 88 I	82	28

[a] C, crystal; Sc*, chiral smectic C phase; S_A, smectic A phase; N* chiral nematic phase; I, isotropic phase. [b] Response time to 10 V/μm electric field at 25 °C in a 2-μm cell.

electric field. The spontaneous polarization causes the orientation of mesogens in the corresponding area to change accordingly.

The maximum gain coefficients of FLCs are plotted as a function of the magnitude of the spontaneous polarization in Figure 10. The formation of the refractive index grating is a process in which the direction of spontaneous polarization of the area between the bright and dark positions of the interference pattern is altered. The formation of the refractive index grating must therefore be affected by the magnitude of spontaneous polarization and the rotational viscosity. As seen in Figure 8, the gain coefficient is dependent on the magnitude of spontaneous polarization. Although the data does not plot on a simple line, there is a tendency for the gain coefficient to be higher in FLCs with larger spontaneous polarization. The deviation may be caused by the difference in rotational viscosity and the homogeneity of the SS state in the samples.

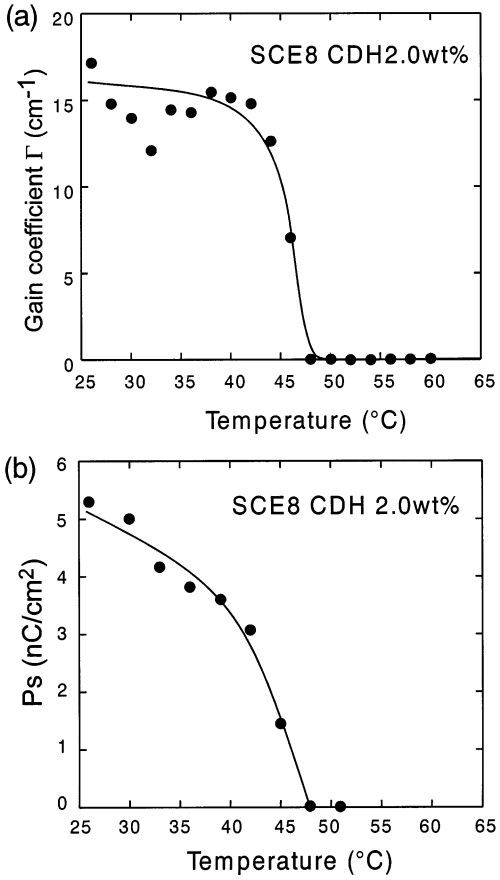

Figure 8. Temperature dependencies of (a) gain coefficient and (b) spontaneous polarization of SCE8 mixed with 2 wt % CDH and 0.1 wt % TNF. For two-beam coupling experiments, an electric field of 0.1 V/μm was applied to the sample. The sample angle α was 50°, and the intersection angle ϕ was 20°.

Effect of the Magnitude of Applied Electric Field. The photorefractive effect in FLCs can be induced by applying a very weak external electric field. The maximum gain coefficient of the SCE8 sample was obtained using an electric field strength of only 0.2∼0.4 V/μm. The dependence of the gain coefficient of FLCs/CDH/TNF on the strength of the electric field is shown in Figure 11. The gain coefficient of SCE8 doped with 0.5∼1 wt % CDH increased with the strength of the external electric field. However, the gain coefficient of SCE8 doped with 2 wt % CDH decreased when the external electric field exceeded 0.4 V/μm. The same tendency was observed for M4851/050. The formation of the orientational grating is enhanced when the external electric field is increased from 0 to 0.2 V/μm as a result of the induced charge separation under a higher external electric field. However, when the external electric field exceeds 0.2 V/μm, many zigzag defects appear in the texture (Figure 12). These defects cause light scattering and a decrease in the gain coefficient.

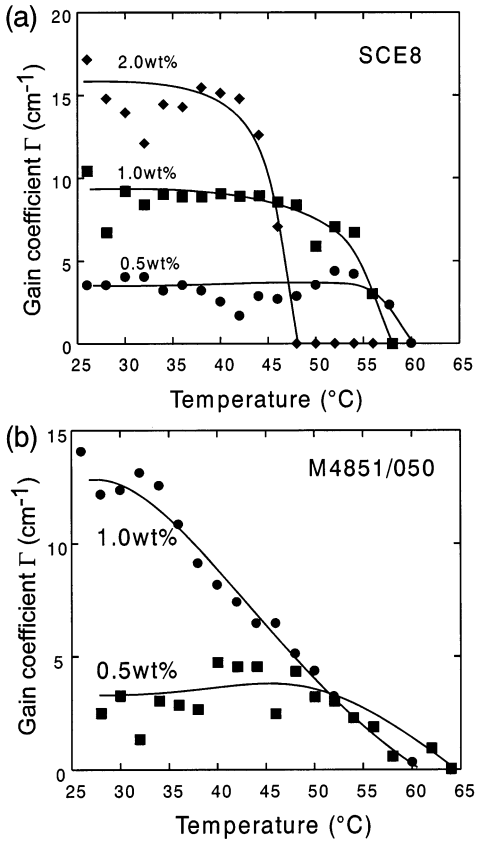

Figure 9. Temperature dependence of the gain coefficient of (a) SCE8 and (b) M4851/050 mixed with several concentrations of CDH and 0.1 wt % TNF. An electric field of 0.1 V/μm was applied to the sample. The sample angle α was 50°, and the intersection angle ϕ was 20°.

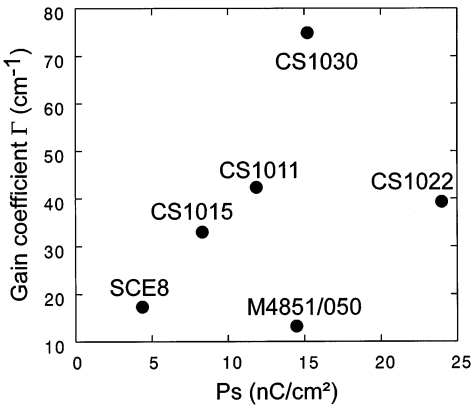

Figure 10. Maximum gain coefficients of FLCs under application of 0.1 V/μm electric field as a function of the magnitude of spontaneous polarization.

Refractive Index Grating Formation Time. The formation of the refractive index grating involves charge separation and reorientation. The index grating formation time is affected by these two processes, and both may be rate-determining steps. The refractive index grating formation times in SCE8 and M4851/050 were measured based on the simplest single-carrier model of photorefractivity,[2] in which the gain transient is exponential. The rising signal of the diffracted beam was fitted by a single-exponential function as follows:

$$\gamma(t) - 1 = (\gamma - 1)[1 - \exp(-t/\tau)] \qquad (2)$$

where $\gamma(t)$ represents the transmitted beam intensity at time t divided by the initial intensity ($\gamma(t) = I(t)/I_0$) and τ is the

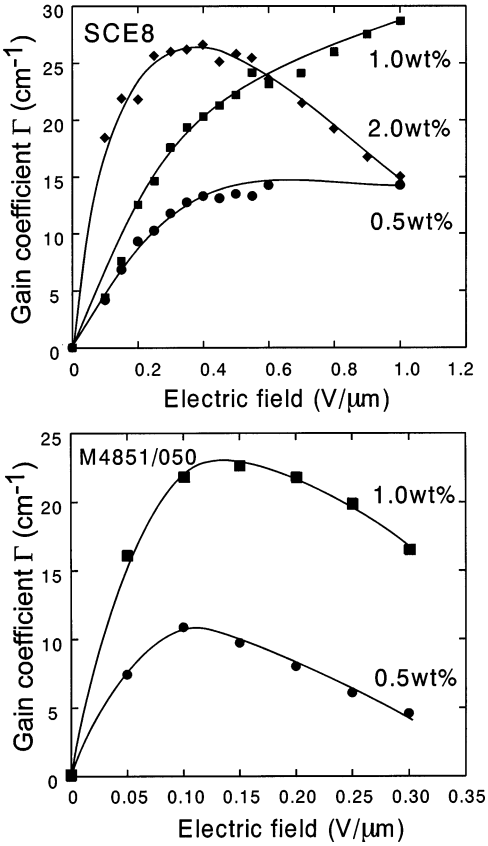

Figure 11. Electric field dependence of the gain coefficient of SCE8 and M4851/050 mixed with several concentrations of CDH and 0.1 wt % TNF in a 10-μm-gap cell measured at 30 °C. The sample angle α was 50°, and the intersection angle ϕ was 20°.

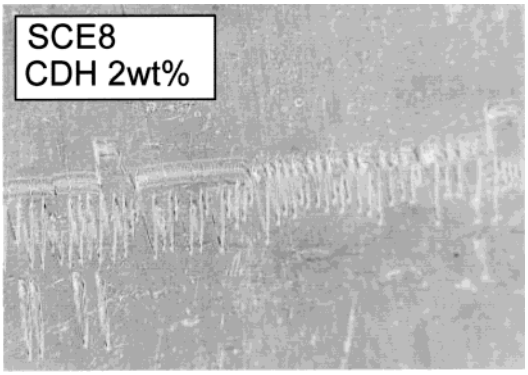

Figure 12. Textures observed in the SS state of SCE8 under applied 0.5 V/μm electric field.

formation time. The grating formation time in SCE8/CDH/TNF is plotted as a function of the strength of the external electric field in Figure 13a. The grating formation time decreases with increasing electric field strength because of the increased efficiency of charge generation. The formation time was shorter at higher temperatures, corresponding to a decrease in the viscosity of the FLC with rising temperature. The formation time for SCE8 was found to be 20 ms at 30 °C. As shown in Figure 13b, the formation time for M4851/050 was found to be independent of the magnitude of the external electric field, with a formation time of 80−90 ms for M4851/050 doped with 1 wt % CDH and 0.1 wt % TNF. This is slower than for SCE8, although the spontaneous polarization of M4851/050 (−14 nC/cm^2) is larger than that of SCE8 (−4.5 nC/cm^2) and the response time of the electrooptical switching (flip of spontaneous polarization) to an electric field (±10 V in a 2 μm cell) is shorter

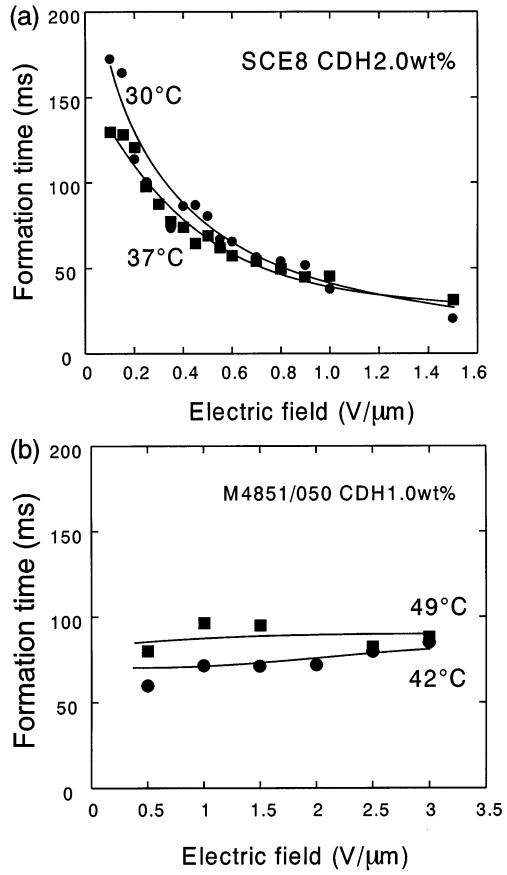

Figure 13. Electric field dependence of index grating formation time. (a) SCE8 mixed with 2 wt % CDH and 0.1 wt % TNF in two-beam coupling experiment. ●, measured at 30 °C ($T/T_{Sc^*-SA} = 0.95$); ■, measured at 37 °C ($T/T_{Sc^*-SA} = 0.97$). (b) M4851/050 mixed with 1 wt % CDH and 0.1 wt % TNF in two-beam coupling experiment. ●, measured at 42 °C ($T/T_{Sc^*-SA} = 0.95$); ■, measured at 49 °C ($T/T_{Sc^*-SA} = 0.97$). The sample angle α was 50°, and the intersection angle ϕ was 20°.

for M4851/050. The slower formation of the refractive index grating must be due to the poor homogeneity of the SS state in M4851/050 and the charge mobility.

Conclusion

The photorefractivity of a series of FLC mixtures was investigated through two-beam coupling experiments. Very fast photorefractive responses (refractive index grating formation time) were obtained in an FLC with homogeneous SS state. The photorefractivity of FLCs was strongly affected by the properties of the FLCs themselves. Besides properties such as spontaneous polarization, viscosity, and phase transition temperature, the homogeneity of the SS state was also found to be a major factor. The gain coefficient, refractive index grating formation time (response time) and stability of the two-beam coupling signal were all affected strongly by the homogeneity of the SS state. Therefore, a highly homogeneous SS state is necessary to create a photorefractive device. The techniques employed recently in the development of fine FLC display panels and defect-free SS−FLC panels[34,35] will be utilized in the future in the fabrication of the photorefractive devices.

Acknowledgment. This study was financially supported by the Casio Science Foundation.

References and Notes

(1) Solymar, L.; Webb, J. D.; Grunnet-Jepsen, A. *The Physics and Applications of Photorefractive Materials*; Oxford: New York, 1996.
(2) Yeh, P. *Introduction to Photorefractive Nonlinear Optics*; John Wiley: New York, 1993.
(3) Moerner, W. E.; Silence, S. M. *Chem. Rev.* **1994**, *94*, 127.
(4) Zilker, S. J. *ChemPhysChem* **2000**, *1*, 72.
(5) Würthner, F.; Wortmann, R.; Meerholz, K. *ChemPhysChem* **2002**, *3*, 17.
(6) Meerholz, K.; Volodin, B. L.; Kippelen, B.; Peyghambarian, N. *Nature* **1994**, *371*, 497.
(7) Volodin, B. L.; Kippelen, B.; Meerholz, K.; Javidi, B.; Peyghambarian, N. *Nature* **1996**, *383*, 58.
(8) Peng, Z.; Bao, Z.; Yu, L. *J. Am. Chem. Soc.* **1994**, *116*, 6003.
(9) Peng, Z.; Gharavi, A. R.; Yu, L. *J. Am. Chem. Soc.* **1997**, *119*, 4622.
(10) Cui, Y.; Swedek, B.; Cheng, N.; Kim, K.-S.; Prasad, P. N. *J. Phys. Chem. B* **1997**, *101*, 3530.
(11) Grunnet-Jepsen, A.; Thompson, C. L.; Moerner, W. E. *Science* **1997**, *277*, 549.
(12) Kippelen, B.; Marder, S. R.; Hendrickx, E.; Maldonado, J. L.; Guillemet, G.; Volodin, B. L.; Steele, D. D.; Enami, Y.; Sandalphon.; Yao, Y. J.; Wang, J. F.; Röckel, H.; Erskine, L.; Peyghambarian, N. *Science* **1998**, *279*, 54.
(13) Meerholz, K.; Nardin, Y. D.; Bittner, R.; Wortmann, R.; Würthner, F. *Appl. Phys. Lett.* **1998**, *73*, 4.
(14) Hendrickx, E.; Wang, J. F.; Maldonado, J. L.; Volodin, B. L.; Mash, E. A.; Persoons, A.; Kippelen, B.; Peyghambarian, N. *Macromolecules* **1998**, *31*, 734.
(15) Hattemer, E.; Zentel, R.; Mecher, E.; Meerholz, K. *Macromolecules* **2000**, *33*, 1972.
(16) Hofmann, U.; Grasruck, M.; Leopold, A.; Schreiber, A.; Schloter, S.; Hohle, C.; Strohriegel, P.; Haarer, D.; Zilker, S. J. *J. Phys. Chem. B* **2000**, *104*, 3887−3891.
(17) Khoo, I. C.; Li, H.; Liang, Y. *Opt. Lett.* **1994**, *19*, 1723.
(18) Rudenko, E. V.; Sukhov, A. V. *JETP Lett.* **1994**, *78*, 875.
(19) Wiederrecht, G. P.; Yoon, B. A.; Wasielewski, M. R. *Science* **1995**, *270*, 1794.
(20) Wiederrecht, G. P.; Yoon, B. A.; Svec, W. A.; Wasielewski, M. R. *J. Am. Chem. Soc.* **1997**, *119*, 3358.
(21) Wiederrecht, G. P.; Waiselewski, M. R. *J. Am. Chem. Soc.* **1998**, *120*, 3231.
(22) Ono, H.; Kawatsuki, N. *Opt. Lett.* **1997**, *22*, 1144.
(23) Goelemme, A.; Volodin, B. L.; Kippelen, B.; Peyghambarian, N. *Opt. Lett.* **1997**, *22*, 1226.
(24) Ono, H.; Kawatsuki, N. *Jpn. J. Appl. Phys.* **1997**, *36*, 6444.
(25) Ono, H.; Kawatsuki, N. *J. Appl. Phys.* **1999**, *85*, 2482.
(26) Ono, H.; Kawamura, T.; Frias, N. M.; Kitamura, K.; Kawatsuki, N.; Norisada, H. *Adv. Mater.* **2000**, *12*, 143.
(27) Wiederrecht, G. P.; Yoon, B. A.; Wasielewski, M. R. *Adv. Mater.* **2000**, *12*, 1533.
(28) Sasaki, T. *Polym. App. (Koubunshi Kakou)* **2000**, *49*, 214.
(29) Sasaki, T.; Shibata, M.; Kino, Y.; Ishikawa, Y.; Yoshimi, T. *Polym. Prepr. Jpn.* **2000**, *49*, 704.
(30) Sasaki, T.; Kino, Y.; Shibata, M.; Mizusaki, N.; Katsuragi, A.; Ishikawa, Y.; Yoshimi, T. *Appl. Phys. Lett.* **2001**, *78*, 4112.
(31) Sasaki, T.; Katsuragi, A.; Ohno, K. *J. Phys. Chem. B* **2002**, *106*, 2520.
(32) Sasaki, T.; Ohno, K.; Nakazawa, Y. *Macromolecules*, **2002**, *35*, 4317.
(33) Skarp, K.; Handschy, M. A. *Mol. Cryst. Liq. Cryst.* **1988**, *165*, 439.
(34) Furue, H.; Miyama, T.; Iimura, Y.; Hasebe, H.; Takatsu, H.; Kobayashi, S. *Jpn. J. Appl. Phys.* **1998**, *37*, 3417.
(35) Takahashi, T.; Furue, H.; Shikada, M.; Matsuda, N.; Miyama, T.; Kobayashi, S. *Jpn. J. Appl. Phys.* **1999**, *38*, 534.